Sun and Geosphere, Vol.4 - No.1 - 2009, in press

A Catalog of Halo Coronal Mass Ejections from SOHO

N. Gopalswamy[1], S. Yashiro[2], G. Michalek[3], H. Xie[3], P. Mäkelä[3], A. Vourlidas[4], R. A. Howard[4]

[1]NASA Goddard Space Flight Center, Greenbelt, Maryland, USA, [2]Interferometrics, Herndon VA, USA, [3]The Catholic University of America, Washington DC, USA, [4]Naval Research Laboratory, Washington DC, USA

Coronal mass ejections (CMEs) that appear to surround the occulting disk of the observing coronagraph are known as halo CMEs. Halos constitute a subset of energetic CMEs that have important heliospheric consequences. Here we describe an on-line catalog that contains all the halo CMEs that were identified in the images obtained by the Solar and Heliospheric Observatory (SOHO) mission's Large Angle and Spectrometric Coronagraph (LASCO) since 1996. Until the end of 2007, some 396 halo CMEs were recorded. For each halo CME, we identify the solar source (heliographic coordinates), the soft X-ray flare importance, and the flare onset time. From the sky-plane speed measurements and the solar source information we obtain the space speed of CMEs using a cone model. In addition to the description of the catalog (http://cdaw.gsfc.nasa.gov/CME_list/HALO/halo.html), we summarize the statistical properties of the halo CMEs. We confirm that halo CMEs are twice faster than ordinary CMEs and are associated with major flares on the average. We also compared the annual rate of halo CMEs with that obtained by automatic detection methods and found that most of these methods have difficulty in identifying full halo CMEs.

1. Introduction

Coronal mass ejections (CMEs) that appear to surround the occulting disk of the coronagraph in white-light coronal images are known as halo CMEs [1]. These are CMEs generally heading towards or away from the observer. CMEs heading away from the observer originate on the backside of the Sun, while those moving towards the observer originate on the visible disk. The Solwind coronagraph on board the P78-1 satellite detected the first halo CME about 20 years ago (1979 November 27). The three-dimensional nature of CMEs became immediately evident from this observation: the CME appeared as a cone projected on the sky plane [1]. The solar source of the CME was a filament eruption located at N05W03. Twenty halos (or 2% out of 998 CMEs) were reported in a subsequent paper [2], but not all of them fully surrounded the occulting disk. With the extended field of view of the Large Angle and Spectrometric Coronagraph (LASCO) on board the Solar and Heliospheric Observatory mission (SOHO), a much larger fraction of CMEs have been found to be halos [3,4]: ~3.6% of all CMEs fully surrounded the occulting disk, while ~11% had widths exceeding 120^o. The Solwind coronagraph, which reported the first statistics on halo CMEs, had a field of view (FOV) of 2.5 - 10 solar radii (Rs), while LASCO has an FOV of 2.5 - 32 Rs. Initially it was thought that CMEs ejected at an angle of 5^o or less with respect to the Sun-Earth line

became halos. The LASCO observations have shown that CMEs originating at larger central meridian distances can also become halos. This is mainly because of the extended FOV of LASCO. In principle, any CME on the disk can become a halo if the coronagraph has infinitely high sensitivity. Figure 1 is a schematic showing three CMEs that become halos when the leading edges are at three different heliocentric distances. Fast and wide CMEs become halos early on (CME labeled 1). The probability of becoming a halo diminishes when the CME is narrow because it has to expand for a long time before being seen above the occulting disk. By the time the CME appears above the occulting disk, it may become too faint to be detected. Thus, whether a CME is observed as a halo or not depends somewhat on the instrument capabilities. The halo CMEs investigated in this paper are identified manually from SOHO/LASCO images.

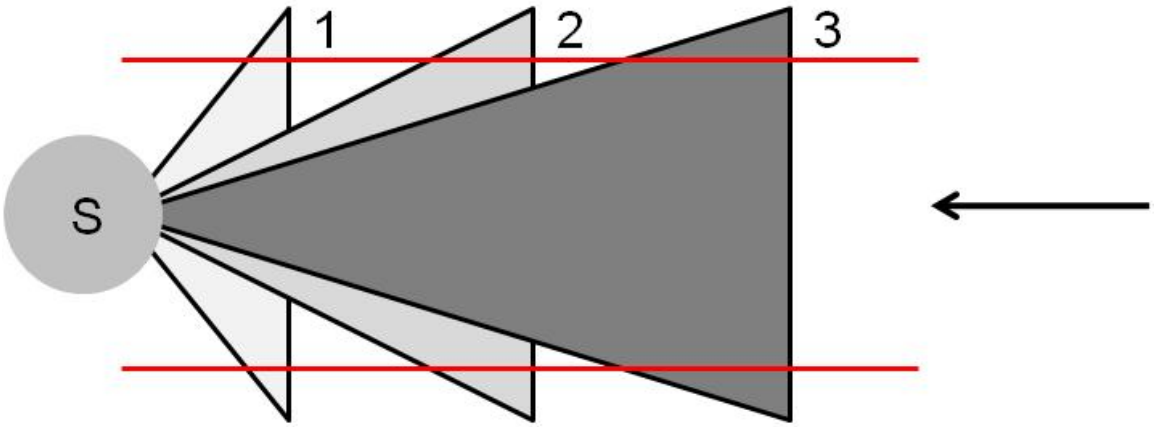

Figure 1.Three CMEs (marked 1, 2, and 3) that would appear as halos when viewed along the direction indicated by the arrow. The two horizontal lines mark the inner edge of the coronagraph FOV because of the occulting disk. Note that only the CME portions outside the two horizontal lines will be seen projected against the sky plane. The leading edges of the CMEs are shown flat for simplicity.

2. Description of Halo CMEs

Full halos refer to CMEs that appear to surround the occulting disk within the coronagraphic field of view [3,5]. CMEs that are wide (width > 120^o, but < 360^o) are known as partial halos. Some researchers collectively refer to all CMEs with ≥ 120^o as halo CMEs. Here we consider only those completely surrounding the occulting disk as full halos. Among full halos, those appearing close to the central meridian either in the frontside or in the backside generally appear symmetric around the occulting disk. Figure 2 shows two halo CMEs, one frontsided with the source identified using an EUV difference image (pointed by an arrow) and the other backsided. Both CMEs have a bright part and a diffuse structure. The diffuse structure can be interpreted as the sheath of the shock driven by the CME. The bright part is the main body of the CME. It is not possible to observe the bright prominence cores in most of the halo CMEs. For the backside CME, the main body of the CME itself forms the halo.

When CMEs originate at a larger central meridian distance (CMD), they appear asymmetric with respect to the occulting disk. The asymmetry can be geometric (outline) or in brightness [3-6]. The frontside CME in Fig. 2 clearly has a brightness asymmetry. The main body of the CME is moving toward Earth with a slight western bias, so the brightness is mostly to the west. The diffuse eastern part must be the disturbance that surrounds the main body of the CME. The outline asymmetry is obvious in CMEs originating from close to the limb (either in front of the limb or behind).

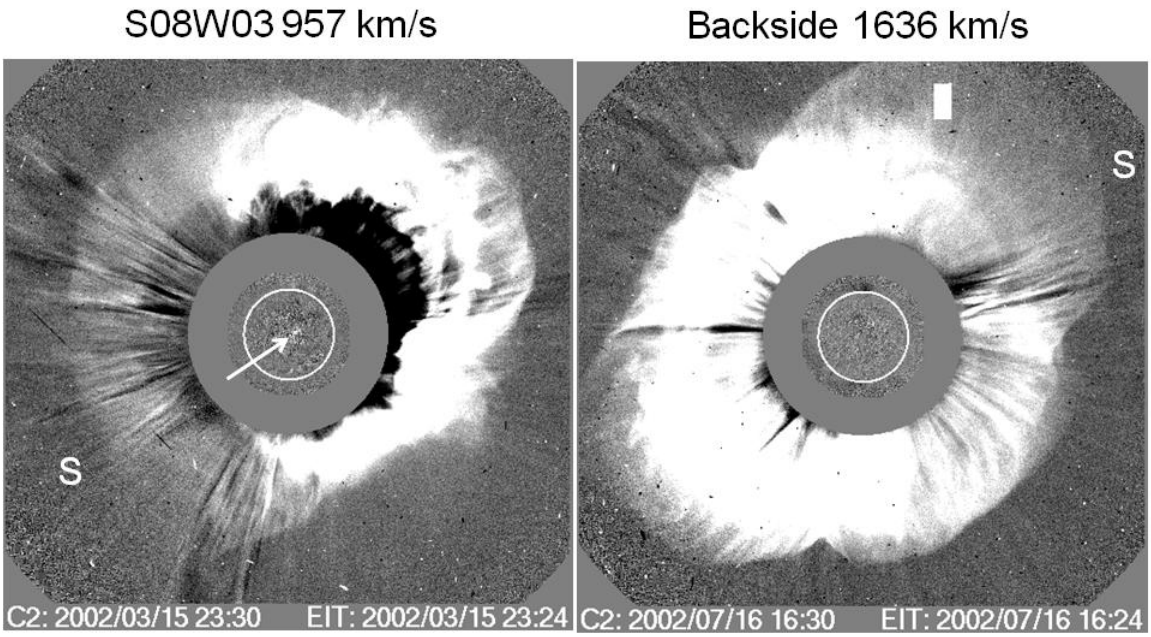

Fig.2. A frontside (left) and a backside halo CME observed in the LASCO/C2 FOV. The coronagraph images are running difference images, which show the change in the corona between successive frames. The coronagraphic images are superposed with EUV difference images from SOHO's Extreme Ultra-violet Imaging Telescope (EIT) that show the changes in the solar disk otherwise blocked by the occulting disk. The arrow points to the source of eruption on the left image (heliographic coordinates S08W03). On the right image, there is no change on the solar disk associated with the CME because the CME originated on the backside of the Sun. There is a hint of this in the EUV difference images, showing dark features all around the limb, except for the northwest part.

In the case of the asymmetric CMEs, what is observed on the limb opposite to that of the source is the disturbance that surrounds the CME. The disturbance is the shock for most of the halo CMEs [7]. Figure 3 shows examples of halo CMEs originating from the east and west limbs. The 2001 December 25 CME in Fig. 3 is labeled "Blimb – SE" because it originated from behind the southeast (SE) limb. Accordingly, the CME leading edge has the largest heliocentric distance in the SE direction (and the least in the northwest (NW) direction). One can also see that the main body of the CME is in the SE direction. We expect that what is observed by the coronagraph is the material behind the sky plane, moving in the anti-earthward direction. The material seen to the north and west must be the disturbance that crossed the solar disk on the backside of the Sun. A similar

explanation applies to the Blimb-SW halo on 2003 November 2. The 2001 December 28 CME originates from the east limb (S24E90) and moves much faster (2216 km/s). The extended flank of the shock is what we see above the NW limb. Both the limb halos in Fig. 3 produced shock signatures along the Sun-Earth line as detected by spacecraft at the L1 point. The shocks were detected on 2001 December 30 at 20:00 UT and 2002 January 17 at 05:50 UT, respectively for the east and west limb halos [8]. In both cases, the shocks were "driverless" because the driving CMEs did not arrive at Earth. In limb events like these, the disturbance on the opposite limb would have traveled both on the front and backside of the Sun away from the region of eruption.

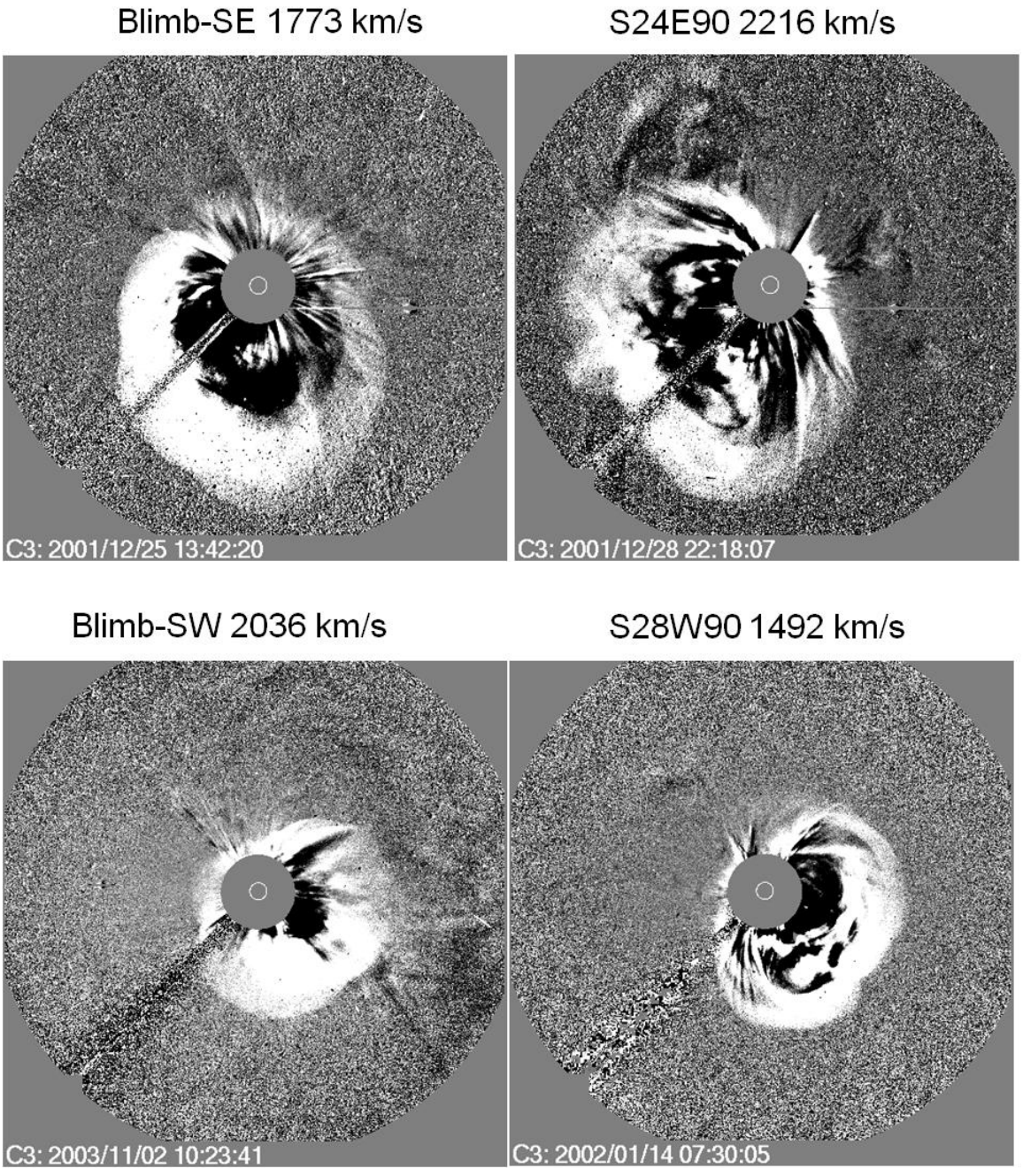

Fig. 3 A behind-the-limb (Blimb) and at the limb halo CMEs from the eastern and western hemispheres. Halos from behind the southeast (SE) and southwest (SW) limbs are shown. The speed and source location are noted in each case.

Some CMEs become halos very early on - in the first or second frame of appearance. These CMEs become full halos in the LASCO/C2 FOV (see Fig. 2). Others become halos only in the C3 FOV. Figure 4 shows a good example. The CME on 2000 April 23 originates from behind the west limb (a Blimb – W event) as indicated by the EUV disturbance pointed by arrows. In the C2 FOV, the CME has an angular width of ~180^{o}, but it further expands and appears as a full halo in the C3 FOV. Note that if there were no C3 coronagraph, this CME would not be classified as a full halo. CMEs that become halos only in the C3 FOV are typically asymmetric.

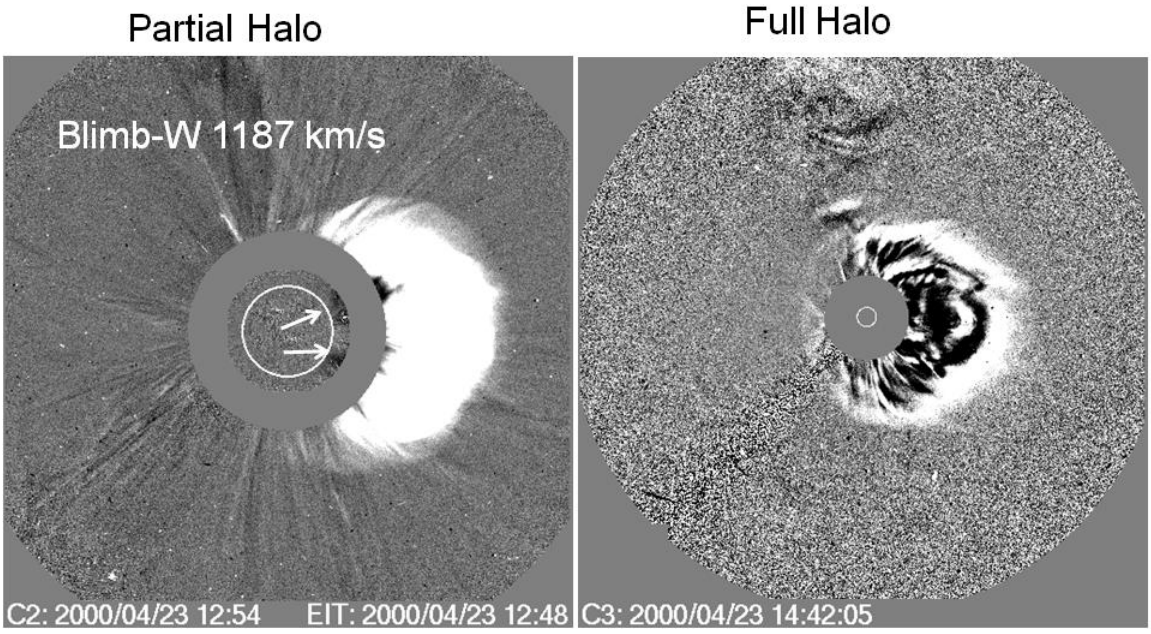

Fig.4. A partial halo CME in the LASCO/C2 FOV becoming a full halo CME in the C3 FOV. The CME originates from behind the west limb as can be seen from the superposed EUV difference image that shows the characteristic signatures of dimming pointed by arrows.

The above discussion illustrates that one needs to know where on the Sun does the CME originate in order to understand the shape of a halo. We have mostly used EIT difference images that show the solar source. Both LASCO and EIT are instruments on board SOHO so the images can be easily superposed and compared. One can also use images at other wavelengths such as soft X-rays, H-alpha, and microwaves to identify the solar source, especially when EIT observations are not available. Figure 5 shows a CME, which became a halo within the C2 FOV. From the LASCO/C2 image shown, it is impossible to tell whether the CME is frontsided or backsided. EIT images were not available for this CME. However, soft X-ray images were available from the Yohkoh satellite. From these images we can readily recognize a post-eruption arcade centered at

the heliographic coordinates N08W18. The arcade structure is consistent with the vertical neutral line in AR 9684 from which the CME erupted. Once the solar source is known, it is easy to understand why the main body of the CME is brighter on the western side.

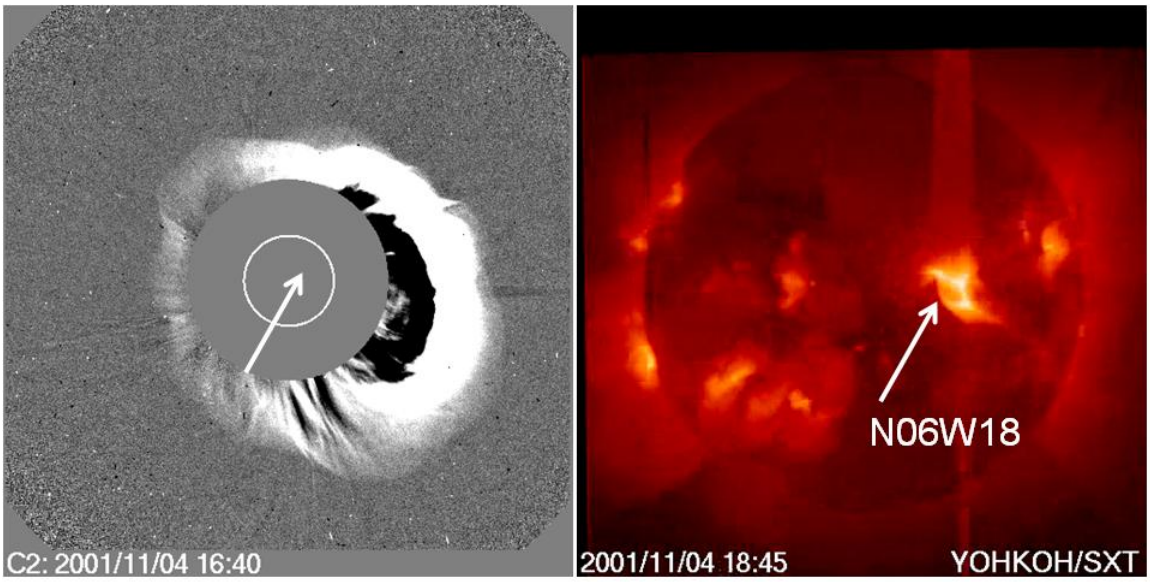

Figure. 5 The frontsided CME of 2001 November 4 at 16:40 UT as observed by LASCO/C2 (left) and its solar source recognized in the soft X-ray image obtained by Yohkoh. The eruption occurred in AR 9684 in association with an X1.0 flare that had a start time of 16:03 UT. The CME first appeared in LASCO/C2 FOV at 16:25 UT and became halo in the next frame at 16:35 UT.

From 1996 to the end of 2007, SOHO detected 396 full halo CMEs. When one includes CMEs with width $\geq 120^{o}$, the number increases to 1248. These numbers are enormous compared to the handful of halos detected by the Solwind coronagraph. As we noted before, the main reason is the enhanced dynamic range, sensitivity, and the extended FOV of the SOHO coronagraphs. This paper is concerned with the full halo CMEs, which are measured and listed in an on-line catalog (http://cdaw.gsfc.nasa.gov/CME_list/HALO/halo.html). We describe the on-line catalog and then summarize the statistical properties of halo CMEs obtained from the catalog.

3. The Halo CME Catalog

The Halo CME Catalog is one of the subcatalogs maintained at the CDAW Data Center. The Halo CME Catalog contains all the full halo CMEs extracted from the general SOHO CME catalog (http://cdaw.gsfc.nasa.gov/CME_list). The overall structure of the halo CME entries is similar to that in the main SOHO/LASCO CME catalog [6,9]. However, significant enhancement has been made by providing additional information such as the CME space speed, solar-source location, flare size, and flare onset time. The solar source and flare information tells us where on the Sun does the halo CME originate. The space speed is the actual speed of the CME, which is needed to understand the CME kinematics in the interplanetary medium.

3.1 Solar Source

The CME source location is primarily defined as the heliographic coordinates of the associated H-alpha flare derived from the Solar Geophysical Data (SGD) listing. If the flare information is not available from the SGD, the source information is obtained from inner coronal images such as Yohkoh/SXT and SOHO/EIT as the centroid of the flare emission (see [10] for details on the CME source identification). Other data such as microwave images from the Nobeyama radioheliograph and H-alpha images are also used when needed. Some solar sources have also been obtained from the Solarsoft Latest Events Archive after October 1, 2002: http://www.lmsal.com/solarsoft/latest_events_archive.html. Note that the flaring region is generally extended, not just the single point given by the heliographic coordinates.

3.2 Space Speed

Coronagraphic images provide information on CMEs projected on the sky plane. The height-time measurements, therefore, are subject to projection effects, except for limb CMEs. Full halo CMEs have their sources generally closer to the disk center, so the measured speeds are not the true speeds. Considering a set of energetic radio-rich CMEs, it was found some time ago that the CME speed depends on the longitude of the solar source [11]. The speeds of the halos also have been shown to have a clear dependence on the longitude of the solar source [10]: the disk and backside halos have roughly the same speed (933 and 832 km/s), while the limb halos are significantly faster on the average (1421 km/s). While there is some selection effect involved (the limb CMEs have to be very fast to become halos) this tendency can be attributed largely to projection effects. Obtaining the actual speed of the CMEs is also important in providing the correct input to the CME/shock travel time models. The earthward speed can be obtained by first obtaining the deprojected speed of the CME and then computing the earthward component.

The space speed of the CMEs have been obtained from a cone model [12], using the sky plane speed, CME width, and the angle made by the CME cone with respect to the sky plane as inputs. The CME width is assumed here to be unknown, and in reality the width is difficult to measure for halo CMEs from near the disk center. We make use of the fact that the CME width depends on the speed reported in [13]: for a set of 341 CMEs that originated within 30° from the limb the CME speed (V in km/s) is related to the width (W in degrees) as $V = 360 + 3.62W$ with a correlation coefficient of 0.69. The observed speed and width in the sky plane are expected to be close to the true speed and width of the CMEs for these limb CMEs. Based on this correlation, we assign an average half width (ω) to each speed range and take it as the cone half angle: 66° ($V_{sky} > 900$ km/s), 45° (500 km/s < $V_{sky} \leq 900$ km/s), and 32° ($V_{sky} < 500$ km/s). The CME space speeds are then calculated from the equation,

$$V_{space} = \frac{\cos\omega + \sin\omega}{\cos\omega\cos\theta + \sin\omega} V_{sky}, \qquad (1)$$

where θ is the angle between the cone axis and the sky plane obtained from the heliographic coordinates of the solar source (see [12] for details). The estimated error is discussed in the Appendix.

3.3 Catalog Entries

The first eight entries in the Halo CME Catalog is shown in Fig. 6. The html table contains eleven columns, describing the key properties of the halo CMEs. The first two columns give the date (yyyy/mm/dd format) and time (UT) of first-appearance of the halo CME in the LASCO/C2 FOV. The first column is linked to the Javascript movie of the halo CME that combines LASCO/C2 difference images superposed on EIT images with the GOES soft X-ray light curves. Such movies are helpful in confirming the solar source and flare association of the CMEs. The second column is linked to the height-time measurements (heliocentric distances with time in UT). The sky-plane speed of the halo CME in km/s obtained using a linear fit to the height-time (h-t) measurements is given in column 3 and linked to a h-t plot in "PNG" format. The fourth column gives the space speed of the CME in km/s, as described in section 3.2. The fifth column gives the CME acceleration obtained from a second order fit to the h-t measurements in the sky plane. The sixth column gives the Measurement Position Angle (MPA) in degrees, measured counterclockwise from the solar north. Even though halo CMEs do not have a central position angle, the h-t measurements are made along the MPA at which the CME seems to be moving the fastest.

First C2 Appearance Date Time [UT]		Apparent Speed [km/s]	Space Speed [km/s]	Accel [m/s^2]	MPA [deg]	Source Location	X-ray Importance	Flare onset [UT]	Daily Movies and Plots	Remarks
1996/04/29	14:38:48	65	----	---	149	Backside?	---	---	C2 C3 SXT PHTX DST Java Movie	Faint; Very Poor Event; Only 2 points; Only C2
1996/08/16	14:14:06	364	----	2.0*1	158	Backside	---	---	C2 C3 195 SXT PHTX DST Java Movie	
1996/11/07	23:20:05	497	497	8.7	114	Blimb-SE	---	---	C2 C3 195 SXT PHTX DST Java Movie	
1996/12/02	15:35:05	538	----	-8.8	253	Backside?	---	---	C2 C3 195 SXT PHTX DST Java Movie	
1997/01/06	15:10:42	136	232	4.1	180	S18E06	A1.1	14:54	C2 C3 SXT PHTX DST Java Movie	
1997/02/07	00:30:05	490	584	14.3	266	S38W31	---	---	C2 C3 195 SXT PHTX DST Java Movie	
1997/04/07	14:27:44	878	1115	3.3	123	S28E19	C6.8	13:50	C2 C3 195 SXT PHTX DST Java Movie	
1997/04/27	10:26:05	280	9998	-0.5	268	Backside	---	---	C2 C3 195 SXT PHTX DST Java Movie	

Fig.6. First eight entries in the Halo CME catalog (cdaw.gsfc.nasa.gov/CME_list/HALO/halo.html). Entries in blue have Hyperlinks to more information.

The solar source location (heliographic coordinates) of the CME is given in column 7. For example, S25E16 means the latitude is 25° south and the longitude is 16° east (source located in the southeast quadrant of the Sun). N denotes northern latitudes and W denotes western longitudes. Entries like Blimb-NE indicate that the source information is not complete, but we can say that the eruption occurs behind the northeast (NE) limb. This information is usually gathered from SOHO/EIT difference images, which show dimming above the limb in question. Completely backside events with no information on the source location are marked as "Backside". A question mark implies less confidence in

the stated position. "---" denotes lack of source information The soft X-ray flare importance (peak flux in the 1-8 Å channel) and the onset time (hh:mm format, date in Column 1 applies) are given columns 8 and 9, respectively. In column 8, "----" means the soft X-ray flux is not available. In column 10, links to various plots and movies associated with the halo are given: C2. C3, 195, and SXT are mpg movies from LASCO (C2, C3), EIT 195, and Yohkoh/SXT. 'PHTX' (proton, height-time, X-ray) is a link to the three-day overview plots of solar energetic particle events (protons in the >10, >50 and >100 MeV GOES channels). 'DST' is a link to the six-day overview plots showing the connection between the halo CME and the Dst index on the one hand and the flare on the other. Finally, column 11 provides notes on the events and the data quality.

4. Statistical Properties

In this section, we provide an over view of the statistical properties of halo CMEs based on those listed in the catalog. We normally refer to this catalog as "Halo CME Catalog". However, we also use the term "CDAW catalog" to distinguish it from other catalogs, in particular those that identify CMEs using computer algorithms (automatic methods). In this section, we discuss the annual occurrence rate, solar source distribution, CME speed, and the flare sizes.

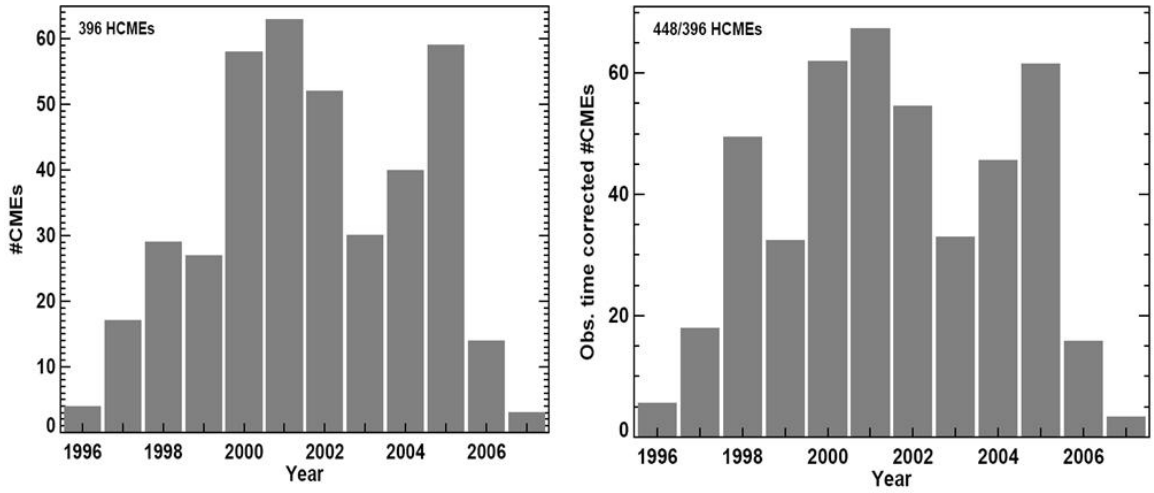

Fig.7. Annual rate of full halo CMEs since 1996 as observed (left) and corrected for down time (right).

4.1 Annual Rate

Figure 7 shows the annual number of halo CMEs exceeded 50 during four years. Three of these years are during the solar maximum and the fourth one is from the declining phase (year 2005). The fraction of time SOHO was making observations ranged from 0.59 (year 1998) to 0.96 (year 2005) with an average value of 0.87. During 1998, there was a data gap of 3 months when SOHO was disabled. Data gaps of 3 hours or more are listed in the main CME catalog [6]. When we corrected for the down time, the annual rate distribution remained roughly the same, except for an increase in the year 1998 by ~20 CMEs. The

corrected total number of halos is 448 instead of the raw count of 396. Both the corrected and uncorrected distributions peak during the solar maximum (year 2001). The peak in the year 2005 is as big as the ones in the solar maximum phase, with ~60 CMEs. In fact, the rate starts increasing in the year 2004 and peaks in 2005. This increase can be attributed to some super active regions that produced a large number of energetic CMEs [14]. The high number in 1998 is also due to a super active region (AR 8210).

The number of full halos identified by automatic detection methods is extremely small compared to the 396 full halos manually identified in the CDAW catalog. Here we compare the CDAW annual rate with that from three other catalogs that automatically detect CMEs: (i) the Automatic Recognition of Transient Events and Marseille Inventory from Synoptic maps (ARTEMIS [15]), (ii) method and the Solar Eruptive Event Detection System (SEEDS [16]) catalog, and (iii) the Computer Aided CME Tracking (CACTus [17]) catalog. Interestingly, ARTEMIS and SEEDS did not detect any full halos! CACTus detected only 50 full halos (only 12.6% of all full halos) over the entire cycle 23. One problem may be that ARTEMIS and SEEDS use the C2 images and many halos form beyond the C2 FOV. However, as we showed in Fig. 2, full halos do form in the C2 FOV itself. Since the full halos cannot be effectively compared, Fig. 8 shows the annual rates of CMEs with widths (W) >120^o and >180^o. Clearly the CDAW and CACTus numbers agree quite well when CMEs with W >180^o and W >120^o are considered, except for the second peak in the in the year 2005. The SEEDS and ARTEMIS show poor agreement with CDAW and CACTus numbers. In the year 2005, the CDAW catalog lists 84 CMEs with W >180^o whereas CACTus detected only 42 such CMEs. SEEDS and ARTEMIS detected only 7 and 3 W >180^o CMEs, respectively in the year 2005. The discrepancies are similar for the >120^o CMEs. Thus the automatic detection of halos seems to be problematic. A detailed examination shows that the automatic methods do identify the halos, but as wide CMEs.

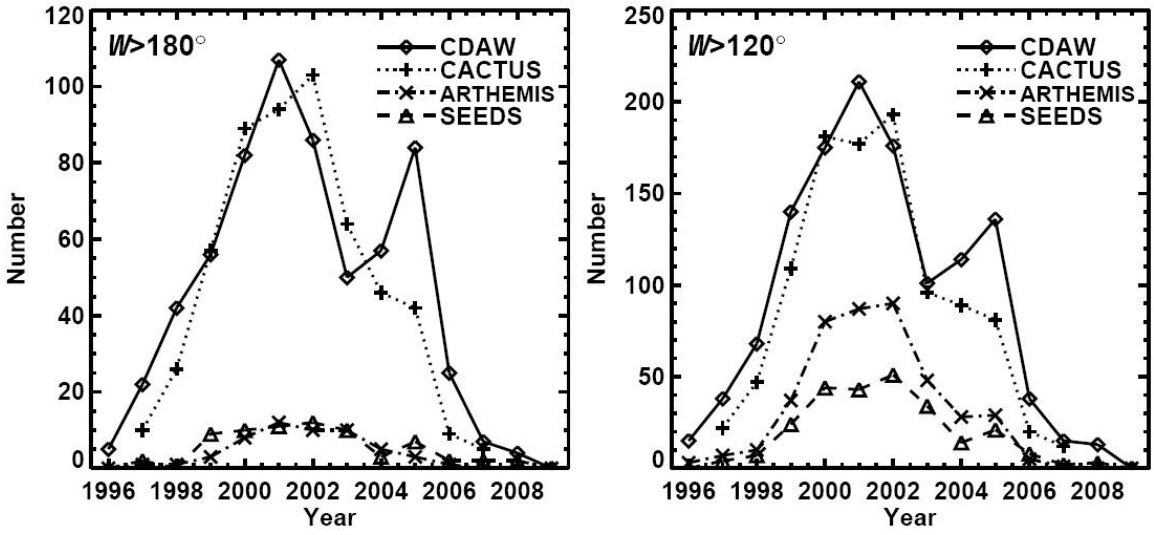

Fig.8. Annual rates of CMEs with width (W) >180^o (left) and >120^o (right). Numbers from the manual catalog (CDAW), ARTEMIS, CACTus, and SEEDS are shown in

different symbols. CACTus and CDAW show reasonable agreement except during the year 2005. The numbers from the other two catalogs are too low.

4.2 Solar Source Distribution

For 247 CMEs, the solar sources are located on the front side of the Sun (see Fig. 9). One can see a clear clustering of CME sources near the central meridian. About 70% of the halos originate within a CMD of 30^o and the remaining ones come from greater CMDs. Examples of limb and disk-center halos can be found in section 2. About 8% the halos originate from the limb (CMD = 90^o). This is the largest angle possible with respect to the Sun-Earth line. The solar sources are also concentrated along $\pm 15^o$ latitudes. Only about ten halos are at latitudes outside the $\pm 30^o$ window. When the latitudes of the solar sources are plotted as a function time, it is found that most of the higher latitude events occur during the rise phase of the cycle (see Fig. 9, right hand side), with a few from the maximum phase. The solar-cycle variation of the source latitudes clearly resembles the sunspot butterfly diagram, suggesting that the halo CMEs primarily originate in the active region belt. This property is common to all the energetic CMEs because the high energy required for the energetic CMEs can be found only in active regions [18]. One can also see a number of clusters of the solar sources, especially during the declining phase. These are due to super active regions.

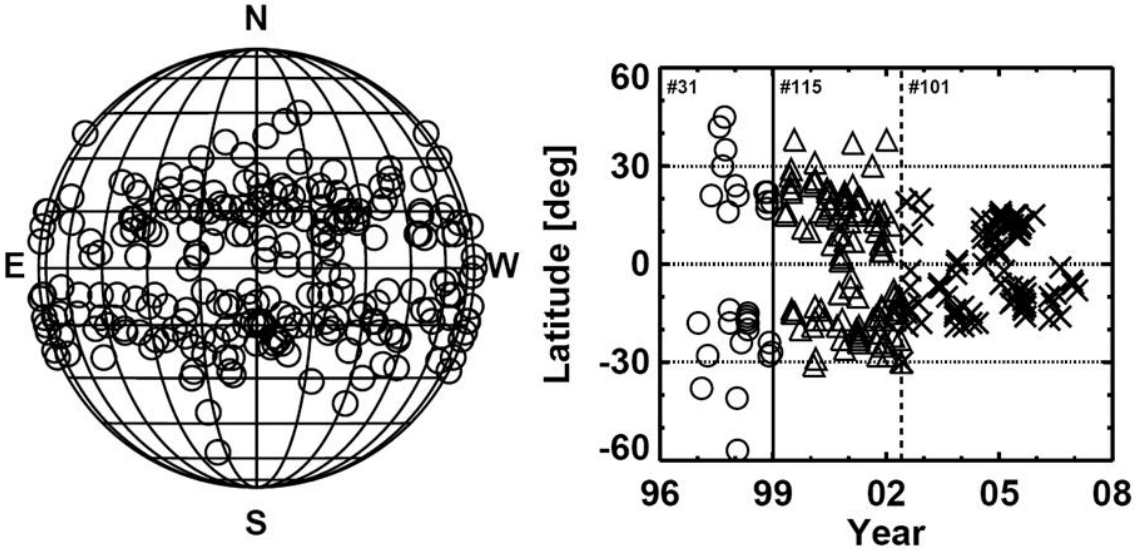

Fig.9. Solar sources of halo CMEs (left) and the source latitudes as a function of time (right). In the right image, the rise, maximum, and declining phases of the solar cycle are distinguished by different symbols. The number of CMEs in each phase of the solar cycle is also shown.

The latitude and longitude distributions in Fig. 10 show the average longitude and latitudes of the solar sources. As in Fig. 9, the number of CMEs drops rapidly beyond a CMD of 30^o. The mean and median values of the longitude distribution are $2^o.7$ and 3^o, respectively. The latitude distribution, on the other hand is bimodal with peaks at $-15^o.8$

and +15°.6 in the southern and northern hemispheres, respectively. These are the average location of the active region belt. The distributions confirm that most of the halo CMEs originate in active regions when the active regions are close to their central meridian passage.

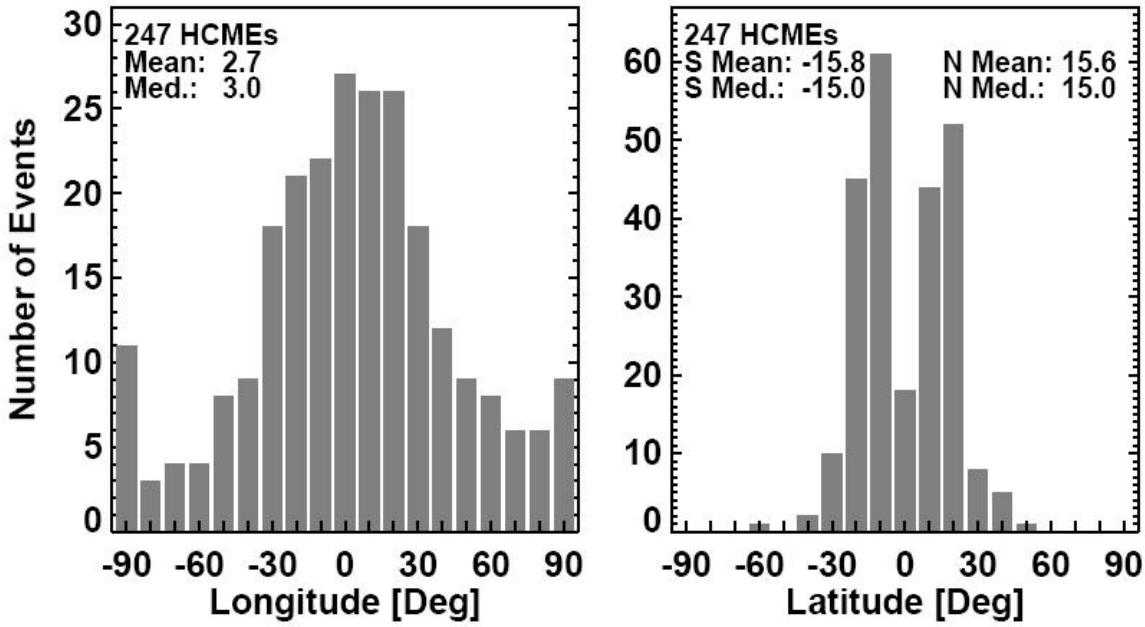

Fig.10. The longitude and latitude distributions of the halo CME source regions. The longitude distribution is clearly centered at the central meridian (mean longitude is W2.7 and median is W03.

4.3 Speed and Flare-size Distributions

It is well known that the halo CMEs are faster on the average [4,10] because of a selection effect of the coronagraph occulting disk that blocks slow and narrow CMEs that do not expand enough to show above the occulting disk within the coronagraphic FOV. As we noted in section 3.2, the sky-plane speeds need to be corrected for projection effects to get the space speed. The projection correction is negligible for limb halos, but it becomes significant for CMD <45°. This is illustrated in Fig. 11, which plots the sky-plane (filled circles) and space (open circles) speeds as a function of the CMD. It is clear that the sky-plane speed increases as a function of the CMD according to $V_{sky} = 750.66 + 10.23L$, where L is the CMD. The correlation coefficient is 0.46, somewhat smaller than the one (0.62) for a set of large CMEs from the rise phase of the cycle [11]. For CMD < 45°, the difference between the sky-plane and space speeds increases. Furthermore, there is no dependence of the space speed on the CMD. Note also that the space speeds do not exceed ~4000 km/s, which has been suggested to be due to the maximum free energy available in solar active regions [18].

Figure 12 shows distributions of the sky-plane and space speeds. The distributions are very similar, with slightly higher values of the mean and median of the space-speed

distribution. The average and median speeds are only ~17% higher for the space speeds. The average sky-plane speed is similar to the past results obtained with different sample sizes [3,4,9,10]. The halo CMEs are inherently wider and hence are of high kinetic energy. The flare-size distribution shown in Fig. 12 is consistent with the high kinetic energy of halo CMEs: the mean and median flare sizes stand at M1.0, compared to just C1.7 for all flares as noted in [10].

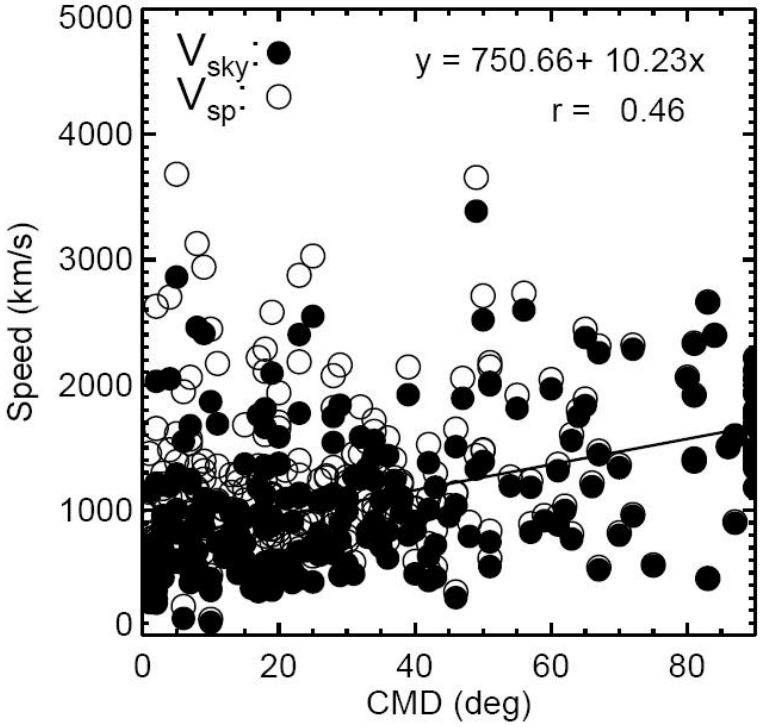

Fig.11. Scatter plot between halo CME speeds (filled circle – sky-plane speed; open circle – space speed) and the central meridian distance (CMD) of the source region on the Sun. The regression line is for the sky-plane speed vs. CMD plot. The equation of the regression line and the correlation coefficient are shown on the plot.

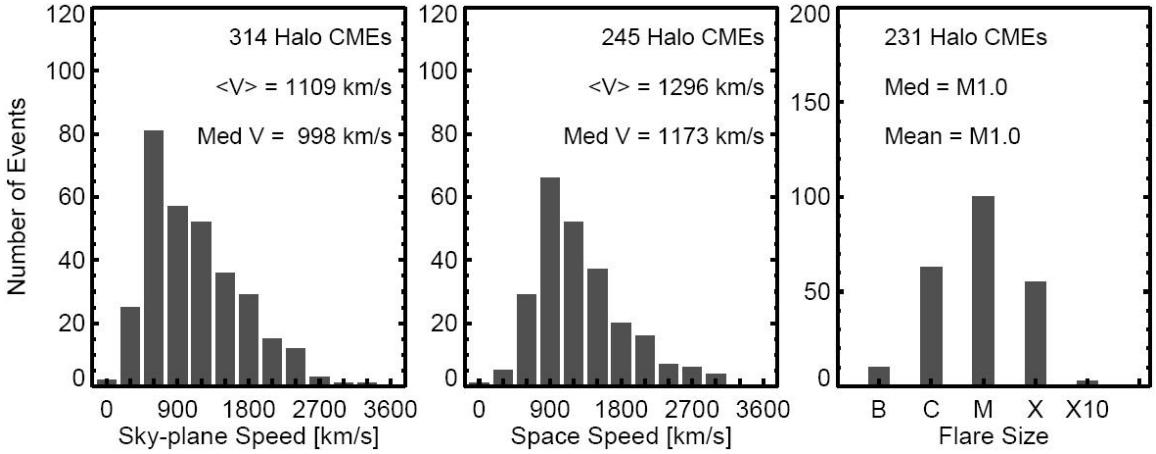

Fig. 12. Distributions of speeds (sky-plane and space) and flare size of halo CMEs. The average and median values of the distributions are shown on the plots.

5. Discussion and Summary

We have described the on-line catalog consisting of halo CMEs manually identified and measured. We also derived several statistical properties of halo CMEs from the 396 events detected by SOHO until the end of 2007. The cataloged events will provide a ready reference for future observations. Note that the full halos constitute only a tiny fraction of all CMEs. Until the end of 2007, SOHO detected 13144 CMEs, of which only 3% are full halos. This number is slightly smaller than earlier estimates using smaller number of CMEs.

It must be pointed out that the definition of halo CMEs does not consider the internal structure of CMEs. It has become increasingly clear that the spatial structure of fast and wide CMEs is more complicated than the traditional three-part structure. Such CMEs are said to have "main body" and an extended diffuse structure surrounding the main body. The extended structure is most likely the shock driven by the main body [19-23]. No attempt was made to separate events that become halos because of the main body or the diffuse structure. When halos are defined by the main body of the CMEs [24], they can be fit extremely well with a full ice cream cone model to establish the relation between radial and expansion speeds [13].

The halos have been shown to be truly high-energy events (the average speed is >1100 km/s compared to ~470 km/s for ordinary CMEs and are expected to be inherently wide). Other studies have shown that the fraction of halo CMEs in a population is indicative of the average energy of the CMEs in the population: shock-driving CMEs, CMEs associated with type II bursts, SEP-producing CMEs, and CMEs resulting in ICMEs detected near Earth (see, e.g., [18]). The fact that halo CMEs are associated with flares of greater X-ray importance further supports the conclusion that halos are very energetic CMEs.

We have not considered the applications of halo CMEs. One obvious example is their ability to cause geomagnetic storms because the CME plasma directly impacts Earth's magnetosphere. The ability and interplanetary structure to produce geomagnetic storms is known as geoeffectiveness. There have been several attempts to characterize the geoeffectiveness (see e.g., [10, 25-28]). When frontsided, ~65% of full halos are geoeffective (Dst ≤ -50 nT) [10]. However, when partial halos are included, only ~40% of the CMEs are geoeffective [28]. Early detection of halo CMEs combined with the estimation of the magnetic field structure and strength is ultimately needed to predict geomagnetic storms, but we are far from this capability.

A final remark is regarding the automatic detection of halo CMEs. It is surprising that the automatic detection techniques miss the majority of halo CMEs, the most important subset of CMEs that have space weather consequences. Thus, the halo CME catalog

serves as an important reference in the process of improving the automatic detection of halo CMEs by computer algorithms.

Appendix: Error Estimation in Space Speed Computation

The errors in the computed space speeds relative to the sky-plane speed (dV_{space}/V_{sky}) are due to measurement errors in the CME cone orientation, $d\theta$, the cone half angular width , $d\omega$, and the sky-plane speed, dV_{sky}. These three errors are given by.

$$dV_{space}/V_{sky} = \frac{1+\tan\omega}{\cos\theta+\tan\omega} dV_{sky}/V_{sky} \qquad \text{(A.1)}$$

$$dV_{space}/V_{sky} = \frac{\sin\theta(1+\tan\omega)}{(\cos\theta+\tan\omega)^2} d\theta \qquad \text{(A.2)}$$

$$dV_{space}/V_{sky} = \frac{(1-\tan\omega^2)(\cos\theta-1)}{(\cos\theta+\tan\omega)^2} d\omega \qquad \text{(A.3)}$$

Figure A.1 shows the errors, dV_{space}/V_{sky}, induced by dV_{sky} (solid curve), $d\theta$ (dotted curve), and $d\omega$ (dashed curve), as function of θ and ω, respectively. In Figure A.1a, the half angular width is set to be ω = 45° and errors are set to be $dV_{sky}/V_{sky} = 0.1$, $d\theta = 0.174$ (rad) (~10°), $d\omega = 0.174$ (rad) (~10°). In Figure A.1b, θ is set to be 90° (in the earthward direction) with the same measurement errors of dV_{sky}, $d\theta$, and $d\omega$.

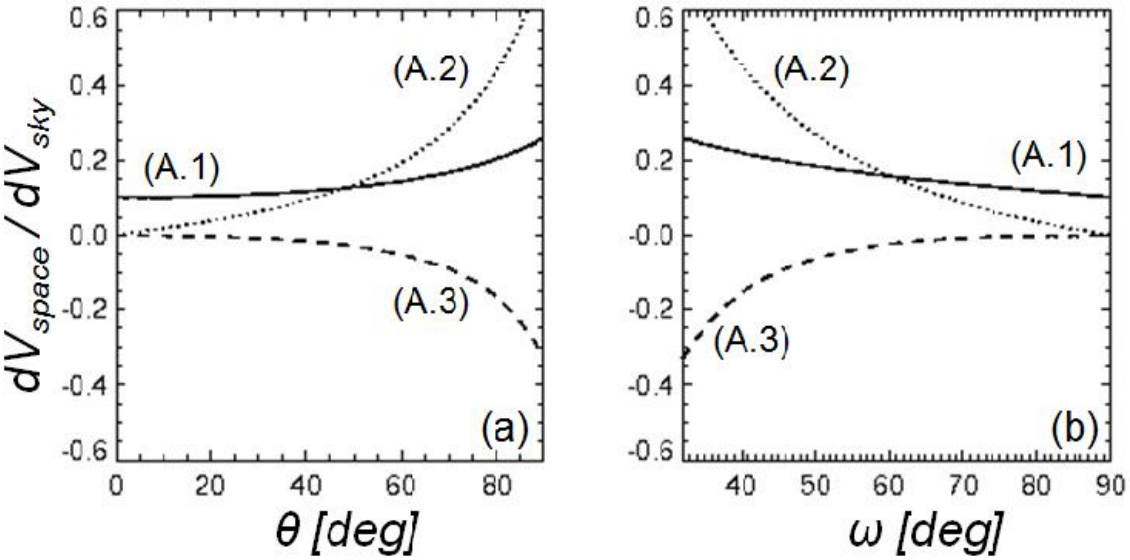

Fig. A.1 Relative error, dV_{space}/V_{sky}, as a function of CME orientation angle θ (left) and half angular width ω (right).

From Figure A.1, we can see that the error caused by dV_{sky} (solid curve) is the smallest among the three curves, which means the measurement error dV_{sky} has relatively small effect on the V_{space} output compared to the errors $d\theta$ (dotted curve) and $d\omega$ (dashed curve). The maximum dV_{space}/V_{sky} for an average ω of 45°and θ of 90° is ~ 0.18 (18%) with dV_{sky}/V_{sky} = 0.1 (10%). As θ approaches 90° (CME originating near the disk center) and ω becomes smaller, the error dV_{space}/V_{sky} due to $d\omega$ and $d\theta$ increase rapidly, and $d\omega$ and $d\theta$ may cause significant errors in the computed V_{space}. The maximum errors of dV_{space}/V_{sky} from $d\omega$ and $d\theta$ can reach 0.6 (60%) and 0.4 (40%), respectively. Thus, for cases when CMEs are very close to the disk center and CMEs having small width, V_{space} output can have relatively large uncertainty.

Acknowledgments
Work supported by NASA's LWS TR&T and VxO programs. SOHO is a project of international cooperation between ESA and NASA.

References

[1] R.A.Howard, D.J.Michels, N.R.Sheeley, Jr., M.J.Koomen, "The Observation of a Coronal Transient Directed at Earth", Astrophys. J., Vol. 263, 1982, L101.
[2] R. A. Howard, N. R. Sheeley, Jr., D. J. Michels, M.J. Koomen, "Coronal mass ejections: 1979– 1981", J. Geophys. Res., vol. 90, 2085, p.8173.
[3] N. Gopalswamy, A. Lara, S. Yashiro, S. Nunes, S., R. A. Howard, in: Wilson, A. (ed.) Solar Variability as an Input to the Earth's Environment SP-535, ESA, Noordwijk, 2003, p.403.
[4] N.Gopalswamy, "A Global Picture of CMEs in the Inner Heliosphere", in: "The Sun and the Heliosphere as an Integrated System", G. Poletto and S. T. Suess (Eds.), Kluwer, Boston, Chapter 8, 2004, p. 201.
[5] O. C. St Cyr, "The Last Word: The Definition of Halo Coronal Mass Ejections", EOS, vol. 86 (30), 2005, p. 281.
[6] N. Gopalswamy, S. Yashiro, G. Michalek, G. Stenborg, A. Vourlidas, S. Freeland, R. A. Howard, "The SOHO/LASCO CME Catalog", Earth, Moon, and Planets, vol. 104, 2009, 295.
[7] N. R. Sheeley, Jr., W. N. Hakala, Y.-M. Wang, "Detection of coronal mass ejection associated shock waves in the outer corona", J. Geophys. Res., vol. 105, 2000, p.5081.
[8] N. Gopalswamy et al., "Interplanetary Shocks Lacking Type II Radio Bursts", Astrophys. J. in press, 2009.
[9] S. Yashiro, N. Gopalswamy, G. Michalek, O. C. St. Cyr, S. P. Plunkett, N. Rich, R. A. Howard, J. Geophys. Res. vol. 109, 2004, A07105.
[10] N. Gopalswamy, S. Yashiro, S. Akiyama, "Geoeffectiveness of halo coronal mass ejections", J. Geophys. Res., vol. 112, 2007, A06112.
[11] N. Gopalswamy et al., "Radio-rich Solar Eruptive Events", Geophys. Res. Lett., vol. 27, 2000, p. 1427.
[12] H. Xie, L. Ofman, G. Lawrence, "Cone model for halo CMEs: Application to space weather forecasting", J. Geophys. Res., vol. 109, 2004, A03109.

[13] N. Gopalswamy, A. Dal Lago, S. Yashiro, S. Akiyama, “The expansion and radial speeds of coronal mass ejections”, Cent. Eur. Astrophys. Bull., vol. 33, 2009, p.115
[14] N. Gopalswamy, S. Yashiro, S. Akiyama, “Coronal mass ejections and space weather due to extreme events”, in: Solar Influence on the Heliosphere and Earth's Environment: Recent Progress and Prospects, N. Gopalswamy and A. Bhattacharyya (Eds.), Quest, Mumbai, 2006, p. 79.
[15] Y. Boursier, P. Lamy A. Llebaria, F. Goudail, S. Robelus, “The ARTEMIS Catalog of LASCO Coronal Mass Ejections”, Solar Phys., vol. 257, 2009, p.125.
[16] O. Olmedo, J, Zhang, H. Wechsler, A. Poland, K. Borne, Solar Phys. 248, p.485
[17] E. Robbrecht, D. Berghmans, Astron. Astrophys., vol. 425, 2004, p. 1097.
[18] N. Gopalswamy, S. Akiyama, S. Yashiro, P. Mäkelä, in "Magnetic Coupling between the Interior and the Atmosphere of the Sun", S. S. Hasan and R. J. Rutten (Eds,) Astrophysics and Space Science Proceedings, Springer-Verlag, Heidelberg, Berlin, 2009, in press.
[19] G. Michalek, N. Gopalswamy, H. Xie,”Width of Radio-Loud and Radio-Quiet CMEs{. Solar Phys. vol. 246, 2007, p. 409.
[20] N. Gopalswamy, et al., “Radio-Quiet Fast and Wide Coronal Mass Ejections”, Astrophys. J., 674, 2008, p. 560.
[21] S. Yashiro, G. Michalek, S. Akiyama, N. Gopalswamy, R. A. Howard, “Spatial Relationship between Solar Flares and Coronal Mass Ejections”, Astrophys. J., vol. 673, 2008, p. 1174.
[22] N. Gopalswamy, “Halo coronal mass ejections and geomagnetic storms”, Earth Planets Space, vol. 61, 2009, p. 595.
[23] V. Ontiveros, A. Vourlidas, “Quantitative Measurements of Coronal Mass Ejection-Driven Shocks from LASCO Observations”, Astrophys. J., vol, 693, 2009, p. 267.
[24] G. Michalek, N. Gopalswamy, S. Yashiro, “Expansion Speed of Coronal Mass Ejections:, Solar Phys., vol. 257, 2009, p. 401.
[25] X. P. Zhao, D. F. Webb, “Source regions and storm effectiveness of frontside full halo coronal mass ejections”, J. Geophys. Res., vol. 108(A6), 2003, p.1234
[26] R.-S. Kim, K.-S. Cho, Y.-J. Moon, Y.-H. Kim, Y. Yi, M. Dryer, S.-C. Bong, and Y. D. Park, “Forecast evaluation of the coronal mass ejection (CME) geoeffectiveness using halo CMEs from 1997 to 2003”, J. Geophys. Res., vol. 110, 2005, A11104.
[27] Yu. I. Yermolaev, M. Yu. Yermolaev, G. N. Zastenker, L. M. Zelenyi, A. A. Petrukovich, J.-A. Sauvaud, “Statistical studies of geomagnetic storm dependencies on solar and interplanetary events: a review”, Planet. Space Sci., vol. 53, 2005, p.189.